In: AIAA Aviation Forum and Ascend 2025, 21-25 July 2025, Las Vegas, USA
DOI: 10.2514/6.2025-3693

Multi-fidelity investigation of low-Reynolds number propeller for different design parameters

Ankit Sharma *, Shubham Shubham †, and Atif Riaz ‡
Cranfield University, Bedford, MK43 0AL, United Kingdom

Anton Ianakiev §
Nottingham Trent University, Nottingham, NG1 4FQ, United Kingdom

This paper presents a comparative multi-fidelity analysis of a small-scale UAV propeller (2-bladed, 0.3m diameter, NACA 4412 airfoil sections) operating at low Reynolds number. Three aerodynamic solvers, high-fidelity Lattice Boltzmann Method (LBM), mid-fidelity lifting-line free vortex wake (LLFVW) and mid-fidelity vortex lattice method (VLM), are evaluated across a broad range of advance ratios, number of blades, collective pitch settings, and skewed inflow angles. All methods predict consistent trends in thrust and torque as design and operational parameters are varied, with the mid-fidelity models closely replicating trends obtained using the high-fidelity LBM. LLFVW generally overestimates and VLM underestimates the magnitudes of thrust and torque relative to experiments (and LBM), but these biases remain approximately constant over the entire range of each parameter. By leveraging these mid-fidelity tools in place of expensive CFD, computational cost is reduced by over two orders of magnitude, with minimal loss of predictive capability. The results demonstrate that mid-fidelity simulations can reliably capture propeller performance trends at a fraction of the CPU cost, making them attractive for rapid design iterations and surrogate-based optimisation frameworks.

I. Introduction

Low-Reynolds-number propellers play a pivotal role in emerging aerospace systems, from unmanned aerial vehicles (UAVs) and micro air vehicles (MAVs) to urban air mobility concepts and small wind turbines. Such propellers operate in a regime where viscous and transitional flow phenomena significantly impact performance [1]. Particularly in the case of MAVs and UAVs, low Reynolds number propellers enable stable and controlled flight in cluttered surroundings, while minimising energy consumption [2, 3]. As the demand for small-scale aerial vehicles continues to rise, the utilisation of low Reynolds number propellers is expected to expand further. Consequently, comprehending the intricate aerodynamic behaviour of such propellers operating at low Reynolds numbers is of utmost importance in order to enhance their performance and efficiency [4, 5]. In this endeavour, a good understanding of the prediction capabilities of different multi-fidelity methods is necessary.

Generally, low-order design tools struggle at low Reynolds numbers, especially for low advance ratios. Large portions of a blade may stall and operate at low Reynolds numbers (Re) beyond the range of standard airfoil data [6]. Blade element models and lifting-line methods often use limited two-dimensional airfoil polars (valid for a narrow angle-of-attack range and a single Re) and neglect rotational augmentation, making it difficult to capture the full performance of low-Re propellers. Macneill et al. [6] extended the blade element methods to better predict the propeller performance operating at low Reynolds numbers. This was done by improving the aerodynamic database of airfoil sections by modifying them to include the effects of rotation across a vast range of Reynolds numbers. These studies also highlight high-fidelity simulations or improved models to reliably design propellers for small UAVs. In that respect, high-fidelity computational fluid dynamics (CFD) has also been employed to study small propellers. Hang et al. [7] used RANS simulations (with a k–ω turbulence model) to analyse propellers at various disk angles (0∘–90∘) and advance ratios up to 0.88, finding good agreement with measured thrust and torque across those conditions. Such CFD studies confirm that capturing three-dimensional unsteady flow features is crucial for accurate performance predictions under inclined flow (skewed inflow) and highlight the need for advanced tools when simpler models become invalid.

*Research Fellow, School of Aerospace, Transport and Manufacturing, ankitsharma@cranfield.ac.uk
†Post-Doctoral Research Fellow, School of Aerospace, Transport and Manufacturing, shubham.shubham@cranfield.ac.uk
‡Senior Lecturer, School of Aerospace, Transport and Manufacturing, a.riaz@cranfield.ac.uk
§Emeritus Professor, Department of Civil Engineering, anton.ianakiev@ntu.ac.uk

Published by AIAA. This is the Author Accepted Manuscript issued with: Creative Commons Attribution License (CC:BY 4.0).
The final published version (version of record) is available online at DOI:10.2514/6.2025-3693. Please refer to any applicable publisher terms of use.

Multi-fidelity design frameworks have emerged as a promising approach to reconcile accuracy and computational cost. In propeller optimisation, low-fidelity models (e.g. BEM or vortex methods) can provide quick evaluations, while periodic high-fidelity simulations serve to correct and inform the lower-fidelity predictions. Toman et al. [8] demonstrated this strategy by coupling BEMT and CFD in a sequential meta-model (surrogate) optimisation of a propeller. Using a space-mapping surrogate with a Kriging response surface, they achieved an optimal blade shape that matched the CFD-optimal solution, while significantly reducing computational expense. This illustrates that mid-fidelity tools, properly calibrated, can drive efficient propeller design with minimal loss in final performance. Pasquale et al. [9] studied leading edge tubercles on propellers using RANS, unsteady viscous vortex panel method, and Lattice Boltzmann Method (LBM). The results showed that for a particular RPM, tubercles which cover the full span of the blades increased the thrust generated. This effect of an increase in thrust rises with an increase in RPM, a trend captured in both experimental and CFD results. Shubham et al. [10] used mid-fidelity lifting line and high-fidelity LBM data combined with a web-based visual analytics framework. The study showed the application of a knowledge generation model for advanced data visualisation techniques, surrogate modelling and optimisation methodologies to handle high-dimensional data across various disciplines, including aerodynamics, aeroacoustics, and structures.

However, there is a notable gap in the literature: while many studies explore propeller design changes with a single numerical method, very few directly compare multiple fidelity levels on the same baseline propeller across a range of operating conditions. A systematic comparison is needed to understand the predictive capabilities and limitations of each approach for low-Re propellers. To address this gap, the present study evaluates three numerical methods of different fidelity. Two mid-fidelity vortex-based solvers – a non-linear lifting-line free vortex wake method (LLFVW) and a vortex lattice method (VLM) – are compared against the high-fidelity Lattice Boltzmann Method (LBM) for the same propeller geometry and conditions. The test case is a 2-bladed, 0.3m diameter propeller (NACA 4412 airfoil sections) previously characterised in experiments [1]. We examine four key design/operational parameters: advance ratio (via varied free-stream velocity at fixed RPM), number of blades, collective pitch angle, and skewed inflow (lateral free-stream component). These parameters span a significant portion of the design space for propellers and represent typical scenarios for small UAV operation (from hover (J=0) up to moderate forward flight (J >0), different prop configurations, blade pitch adjustments, and crosswind inflow).

By analysing each parameter's effect on thrust and torque using LBM, LLFVW, and VLM, we assess how well the lower-fidelity models capture the physics relative to the high-fidelity baseline. The overarching goal is to determine whether mid-fidelity methods can serve as reliable surrogates for high-fidelity CFD in low-Reynolds-number propeller design. If the mid-fidelity solvers can predict performance trends accurately across these diverse conditions, it would justify their use in rapid design loops and multi-fidelity optimisation strategies, with high-fidelity simulations reserved for final validation or calibrating the mid-fidelity models. This paper thus contributes a comprehensive comparison of propeller aerodynamic predictions at multiple fidelity levels, offering guidance on the trade-offs between computational cost and accuracy for low-Re propeller analysis.

The paper is structured as follows. Section II discusses the mid-fidelity and high-fidelity methodologies used in the multi-fidelity framework. Section III discusses the propeller geometries, numerical setup of the mid-fidelity and high-fidelity simulations, and operational and design conditions simulated. Section IV reports the latest results for aerodynamic performance and flow visualisation. Finally, Section V discusses the conclusions of the study and recommendations for future studies.

II. Methodology

A. Flow solver: mid-fidelity LLFVW

The lifting line free vortex wake (LLFVW) method is used to compute the force and flow field, using the open-source software QBlade 2.0 [11], because it was shown to be accurate and efficient for similar low Reynolds number rotor applications [12–14]. The lifting line method belongs to a family of various "vortex methods", the computational cost of which falls somewhere in between low-fidelity momentum methods (BEMT, DMS, etc.) and high-fidelity CFD methods (Navier-Stokes, Lattice-Boltzmann). In the present study, the lifting line theory coupled to a free vortex wake model is used to calculate the propeller three-dimensional (3D) unsteady flow field past the rotor and the interaction between the blade and fluid flow [15, 16]. The LLFVW algorithm is based on a nonlinear lifting line formulation by Garrel [17] and is mentioned in detail by Balduzzi [16].

The fluid is modelled as incompressible, inviscid and irrotational; the blade is modelled with a single line of vortices, which is located on the quarter chord points of the blade. The wake is discretised into vortex line elements (straight or

curved), and these elements are shed at the blade trailing edges at every time step. They then undergo free convection past the rotor ("free wake method") in which the position of the wake end nodes is updated based on the local velocity, which is a combination of the inflow velocity and induced velocity from all the wake elements in the domain. Nonlinear in the "nonlinear lifting line formulation" means the circulation calculated on the lifting line bound vortices is acquired from the nonlinear airfoil lift and drag data provided as input. Lift and drag forces are then calculated based on the local angle of attack (α).

The vortex elements are desingularised using the van Garrel's cut-off method [18] with the vortex core size, taking into account viscous diffusion via the vortex core size that is modelled through the kinematic viscosity ν, a turbulent vortex viscosity coefficient δ_v, and a time offset parameter S_c using the below equation:

$$r_c = \left(\frac{5.03 \delta_v \nu \, (t + S_c)}{1 + \varepsilon} \right)^{1/2} \tag{1}$$

The effects of unsteady aerodynamics and dynamic stall are introduced via the ATEFlap aerodynamic model [19, 20] that reconstructs lift and drag hysteresis curves from a decomposition of the lift polars. The implemented ATEFlap formulation has been further adapted to work under the complex conditions of a propeller exhibiting large fluctuations in the angle of attack when rotating at low TSR [21]. Wake reduction schemes have been implemented to lower computational requirements [19–22].

B. Flow solver: mid-fidelity VLM

The aerodynamic analysis is then performed using VSPAERO, an aerodynamic solver integrated with the NASA Open Vehicle Sketch Pad (OpenVSP) geometry definition tool [23], which solves the potential flow field about these surfaces using a Vortex Lattice Method. The VLM discretises lifting surfaces into a lattice of bound vortex filaments, enabling a mid-fidelity, inviscid flow solution for lift, induced drag, and pressure distributions [24].

A rotating blade approach was used where each propeller blade is explicitly modelled as a lifting surface defined by its geometric parameters (twist, chord, and airfoil shape). The blades are represented using vortex lattice elements, and their positions are updated at each time step to reflect actual physical rotation. The wake filaments shed by the blades are also propagated in time, capturing the inherently unsteady nature of the flow [25].

This time-accurate, unsteady analysis is performed by advancing the solution through multiple blade revolutions until a periodic flow pattern emerges. The method can capture transient phenomena such as blade-vortex interactions, wake distortion, and load fluctuations throughout each revolution. Consequently, this approach provides a higher-fidelity representation of the propeller flow physics but is more computationally expensive because of the need for fine temporal discretisation and multiple time steps compared to actuator disk methods.

C. Flow solver: high-fidelity LBM

The Lattice Boltzmann Method (LBM) is used to compute the flow field because it was shown to be accurate and efficient for similar low Reynolds number rotor applications [26–28]. The commercial software 3DS Simulia PowerFLOW has already been validated for aerodynamic and aeroacoustic studies on propellers in general [9, 29–32]. The software solves the discrete Lattice Boltzmann (LB) equation for a finite number of directions. For a detailed description of the method, the reader can refer to Succi [33] and Shan et al. [34], while to Chen and Doolen [35] for a review. The LB method determines the macroscopic flow variables starting from the mesoscopic kinetic equation, i.e. the LB equation. The discretisation used for this particular application consists of 19 discrete velocities in three dimensions (D3Q19), involving a third-order truncation of the Chapman-Enskog expansion [36]. The distribution of particles is solved by means of the LB equation on a Cartesian mesh, known as a lattice. An explicit time integration and a collision model are used. For the collision term, the formulation based on a unique Galilean invariant [37] is used. The equilibrium distribution of Maxwell-Boltzmann is adopted [36].

To take into account the effect of the sub-grid unresolved scales of turbulence, a Very Large Eddy Simulation (VLES) model is implemented. Following Yakhot and Orszag [38], a two-equations $k - \epsilon$ Renormalization Group is used to compute a turbulent relaxation time that is added to the viscous relaxation time. To reduce the computational cost, a pressure-gradient-extended wall-model is used to approximate the no-slip boundary condition on solid walls [39, 40]. The model is based on the extension of the generalised law-of-the-wall model [41] to take into account the effect of pressure gradient. These equations are iteratively solved from the first cell close to the wall in order to specify the boundary conditions of the turbulence model. For this purpose, a slip algorithm [35], obtained as generalisation of a bounce-back and specular reflection process, is used.

III. Numerical setup

A. Propeller geometry

The baseline propeller geometry used is a two-bladed rotor and employs the NACA4412 airfoil profile throughout the blade span starting from 0.2 to 1 r/R, which is consistent with the propeller geometry used in Casalino et al. [1]. The blade geometry, shown in Fig. 1, is made up of 120 blade sections with varying twist and chord lengths with radial distance. The propeller has a diameter of (D = 0.3 m), rotor diameter (tip radius R_T = 0.15 m), and a root section that transitions from a NACA0012 airfoil at a radius of 1cm (r/R_T = 6%). The hub radius is 1.25cm.

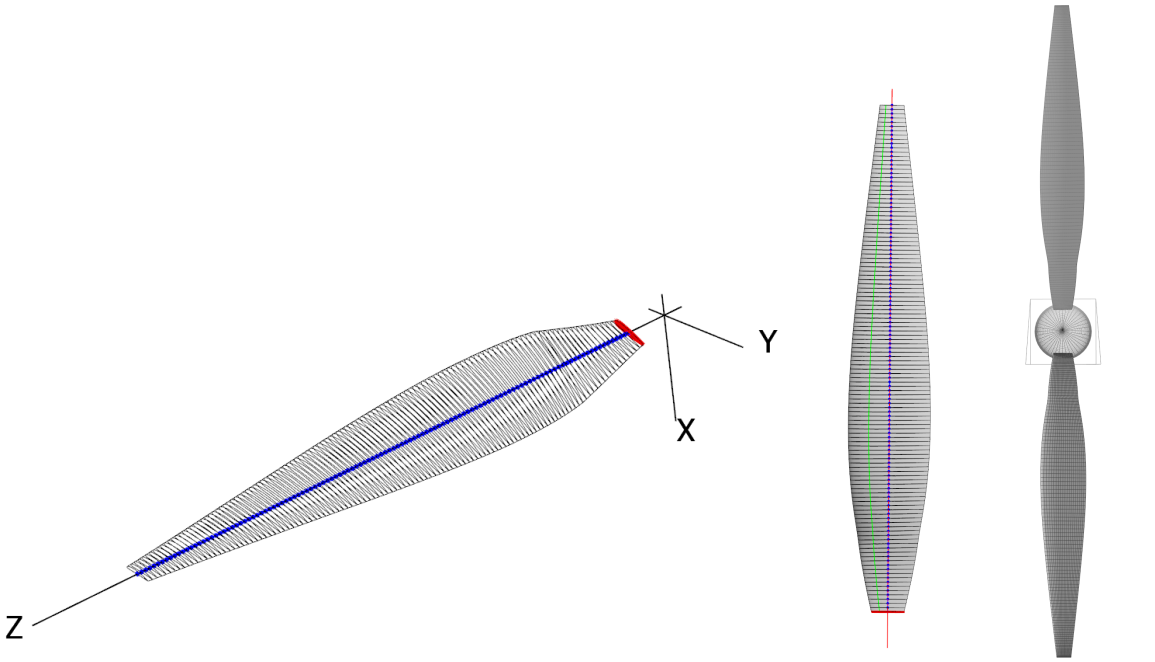

(a) Isometric view (b) Top view (c) 2-bladed propeller

Fig. 1 Baseline propeller geometry

Table 1 lists down all the design configurations simulated in this study. First is the baseline propeller, which is the same as the original propeller geometry and will be used to experimentally validate the current results. Four different design and operational parameters are studied - freestream velocity, number of blades, pitch angle and skewed inflow (lateral velocity in the plane of propeller rotation). These design parameters encompass a significant part of the 3D design space of propeller design. Therefore, the results obtained are expected to provide a very good understanding of the prediction capabilities of each multi-fidelity method used in this study, over a vast range of design configurations.

The present study utilizes all three high-fidelity LBM, mid-fidelity LLFVW and VLM simulations for the baseline propeller geometry and for all different design configurations. To ensure accurate results with both low and mid-fidelity methods, precise airfoil data is essential. To obtain lift and drag coefficients, XFoil [42] is employed for Reynolds numbers ranging from 1×10^5 to 5×10^6. The XFoil calculations utilize an *NCrit* value of nine and natural transition at both the pressure and suction side. The airfoil's static polar data is extrapolated to a 360° range of angle of attack (AoA) using the Montgomerie method [43] to ensure a smooth extrapolation in the post-stall regime. Balduzzi et al. [16] provide an example of the 360° extrapolated polars using the same method.

B. Computational setup

In the high-fidelity LBM approach, a simulation volume is employed, characterized as a cube with all sides measuring $100D$. This volume encompasses the propeller geometry, which is centrally positioned within the domain. The corresponding boundary conditions are illustrated in Figure 2 (a). Specifically, the velocity inlet is set to the

Table 1 Different design configurations simulated in this study

Parameter	Freestream velocity, V_∞ [m/s]	Number of blades	Pitch angle	Lateral velocity, V_L [m/s]
Baseline	0	2	0	0
Velocity	**6**	2	0	0
Velocity	**10**	2	0	0
Velocity	**15**	2	0	0
Velocity	**20**	2	0	0
Blades	0	**3**	0	0
Blades	0	**4**	0	0
Blades	0	**5**	0	0
Pitch	0	2	**2.5**	0
Pitch	0	2	**5**	0
Pitch	0	2	**7.5**	0
Pitch	0	2	**10**	0
Lateral Velocity	10	2	0	**2.5**
Lateral Velocity	10	2	0	**5**
Lateral Velocity	10	2	0	**7.5**
Lateral Velocity	10	2	0	**10**

freestream velocity V_∞ along the X-axis, while a constant ambient pressure of 101.325 kPa is imposed at the pressure outlet. Additionally, the blade surface adheres to a no-slip boundary condition. To facilitate the generation of a computational grid, PowerFLOW utilizes a Cartesian volume mesh encompassing the individual solid components within the simulation domain. This process commences with the smallest hexahedral cell (voxel) size and incorporates a specified number of variable resolution (VR) levels. The VR levels are organized in a fine-to-coarse sequence, with a voxel size change factor of 2 between adjacent VRs, resulting in distinct VR regions. The software automatically intersects the Cartesian mesh with the solid components, thereby generating a collection of polygons known as surfels, which accurately represent the body's surface geometry.

In order to enhance computational efficiency, the present study employs 17 VR regions. These regions feature higher resolutions in proximity to the blade surface, incorporating an offset, while the coarser regions are positioned further away from the blade and rotor. This strategic allocation of computational effort prioritizes areas of interest and regions expected to exhibit significant flow gradients, thus optimizing the simulation process.

In Figure 2 (a) and (b), three red spherical surfaces are depicted, enclosing the rotor flow field. These surfaces serve as Ffowcs Williams-Hawkings (FW-H) permeable surfaces, aimed at mitigating hydrodynamic fluctuations originating from the propeller wake vortices. By averaging the pressure data collected from these permeable surfaces, the presence of spurious noise sources can be diminished. The blade surfaces of the propeller are identified as FW-H solid surfaces. Although FWH surfaces are implemented in the computational setup, the aeroacoustic results are not reported in this study and will be presented in future investigations.

For the mid-fidelity LLFVW simulation, Table 2 outlines the values of the simulation parameters utilised, which have been adopted from a previously validated setup by Shubham et al. [45] for a similar low Re rotor application.

For mid-fidelity VLM, the propeller geometry is created by defining the number of blades, diameter and radial distributions of chord, twist and airfoil sections. The Beta 3/4 value was defined as 15.695 degrees. Flight conditions were defined such as V_∞ as 0 m/s for hover and V_{ref}, which is the rotor tip velocity, as 78.54 m/s and $Mach_{ref}$ as 0.24. A total of 1800 blade panels, 64 wake nodes, and a time step of 0.0005 sec are used.

C. Flow conditions and grid settings

Table 3 presents the operational settings of the baseline propeller in the context of both the mid-fidelity and high-fidelity methods employed in the current study. The system's operational state is characterized using the Advance Ratio (AR) as a metric. The AR is defined as the ratio of the freestream velocity to the propeller tip speed and is denoted

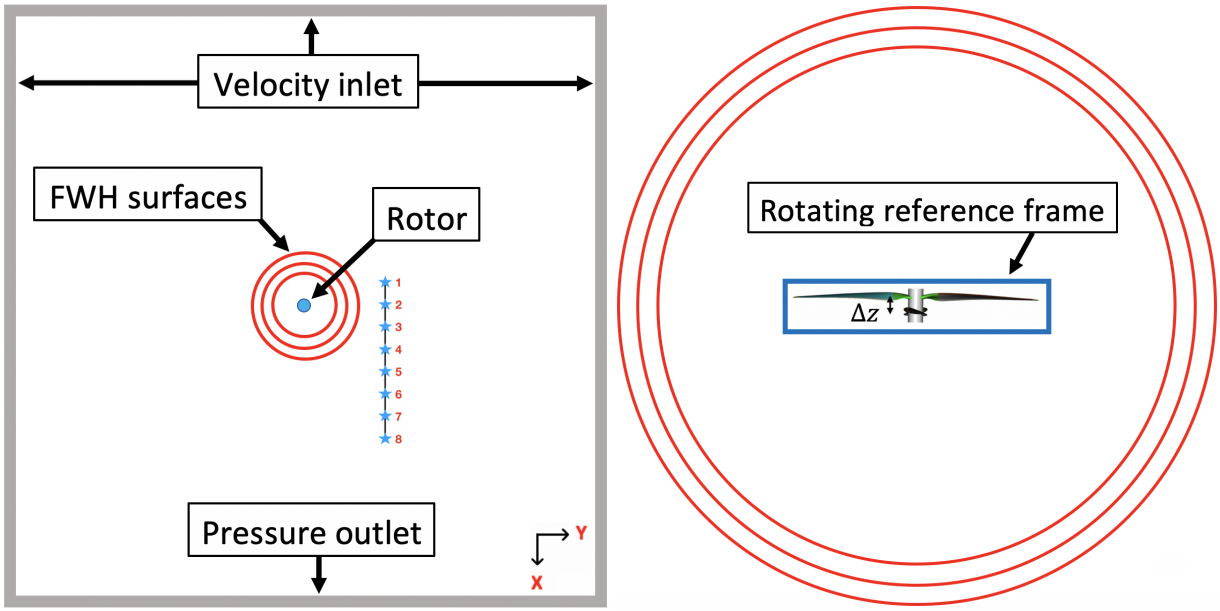

(a) Full computational domain

(b) Zoomed-in view near the propeller

Fig. 2 Numerical setup (adapted from Shubham et al. [44])

Table 2 Simulation parameters used for the LLFVW method

	LLFVW
Freestream velocity V_∞	0 m/s
Density	1.225 kg/m^3
Kinematic viscosity	1.65 e-5 m^2/s
Blade discretization	120 (cosine)
Azimuthal discretization	3 deg
Full wake length	12
Vortex time offset	1 e-4 sec
Turbulent vortex viscosity	50

as J: (V_∞/nD), where V_∞ represents the freestream velocity, n rotations per second and D the propeller diameter. All other operational and design parameters simulated in this study are listed in Table 1.

Table 3 Baseline propeller operational settings for all different methods used

Parameter	
Freestream velocity (V_∞)	0 m/s
Advance ratio (J)	0
Rotations per minute (RPM)	5000
Minimum Reynolds number ($Re_c min$)	4.64e4
Maximum Reynolds number ($Re_c max$)	9.67e4

The freestream turbulence intensity (I_t) and turbulence length scale (L_t) are both set to 0.1% and 1 mm, respectively. However, it is anticipated, based on prior research by Casalino et al. [30], that these parameters will not significantly influence the evolution of the unsteady flow field.

The current high-fidelity setup and grid configuration employed in this study are based on the study conducted by Casalino et al. [1]. The previous study extensively tested various grid sizes, and the chosen setup has been adopted as it has demonstrated satisfactory performance. In the finest VR, the values of y+ and voxels per chord are determined to be 30 and 2.7 $\times 10^2$, respectively. The y+ value represents a dimensionless parameter indicating the distance of the first cell centre from the computational domain's wall in the wall-normal direction. In the present study, it is computed based on the rotational velocity experienced by the blade at the mid-span location. The voxels per chord parameter, on the other hand, signifies the number of grid cells along the chord direction of the blade and is also evaluated at the blade mid-span location. It is important to note that these grid parameters have been carefully selected and optimized to ensure accurate and efficient simulations in the current investigation, leveraging the knowledge and findings from a previous study on co-rotating propellers [28, 46].

The voxel size corresponding to the finest VR used in the baseline propeller configuration is 0.315 mm. Within the computational domain, the number of fine equivalent voxels is 30.94 million. These fine equivalent voxels are obtained by multiplying the number of voxels by the time stepping rate, which is directly linked to the mesh resolution level. Importantly, doubling the voxel size results in a computational cost reduction of half, as the time step is also doubled accordingly. For the simulations performed in this study, the computational effort is quantified in CPU hours and amounts to 2.01e4 for the simulation of 12 rotor rotations (0.144 secs at 5000 RPM). The high-fidelity simulations were executed on a Linux workstation equipped with an AMD Ryzen Threadripper 3990X Gen3 64 Core 128GB DDR4 3GHz platform. In terms of temporal discretisation, the physical time step corresponding to the grid used ensures a Courant-Friedrichs-Lewy (CFL) number of 1 in the finest VR level. Consequently, the time step values are determined to be 1.51×10^{-6} s.

IV. Results

Statistical temporal convergence characteristics of the thrust coefficient (C_T) and the torque coefficient (C_Q) for the baseline configuration are shown in Figure 3. C_T is obtained by dividing thrust value with $\rho n^2 D^4$ and C_Q is obtained by dividing torque value with $\rho n^2 D^5$, where, ρ is density, n is rotations per second and D is propeller diameter. These results are obtained using all three high-fidelity LBM and mid-fidelity LLFVW and VLM methods. The corresponding uncertainty values (u) are calculated as a percentage of the standard deviation of thrust and torque values after the 4th rotor rotation for high-fidelity and after the 8th rotor rotation for mid-fidelity. These uncertainty values reflect the degree of uncertainty or variability in the computed thrust and torque coefficients over time due to the inherent unsteadiness and randomness in the fluid dynamic interactions.

It is evident that the results obtained from the high-fidelity LBM converge after at least 4 rotations, while the results for both mid-fidelity methods converge after 8 rotations. The results for thrust show more unsteady variations than torque for all the numerical methods employed (except for VLM). Furthermore, the highest uncertainty in convergence values is found with mid-fidelity VLM values and the lowest is found with high-fidelity LBM values. To ensure that statistical convergence is achieved for all parameters, all subsequent results in this study are derived from the 6th rotation for the high-fidelity method and the 10th rotation for both mid-fidelity methods.

Figure 4 compares the high-fidelity and mid-fidelity results from the current study and the reference results ("Experiments-ref" and "LBM-ref") by Casalino et al. [1] for a range of advance ratios. The reference data consists of the experimental measurements for the propeller in a wind tunnel and high-fidelity LBM. A very good overall agreement is observed between LBM, LLFVW, VLM and the reference results, for both thrust and torque. There is a slight deviation observed for LBM values in the case of torque results at high J (0.6-0.8), where LBM predicts lower values than the spread of values for other methods. For both thrust and torque, VLM slightly under-predicts as compared to experiments. Overall, the trend observed is consistent amongst all methods used, including reference experimental results, over the full range of advance ratios. Consequently, the current numerical setups are deemed sufficient to enable an accurate and insightful physical analysis of the fluid dynamic interactions and to compare the prediction capabilities of different numerical methods over a varied range of design configurations.

Figures 5 and 6 report the results for thrust and torque variation with number of blades and pitch angle, respectively. Both results show a consistent increase in values as either parameter value is increased, at a constant RPM of 5000. LLFVW predicts higher values than LBM results, which is also observed in the case of variation in the advance ratio. In case of pitch angle, VLM agrees much better with LBM, which is lower than LLFVW values. For some design points, VLM values are not shown since the solution became unstable and gave NaN values. This will be investigated in future studies. Nevertheless, there is a constant difference in predicted values between all the different methods used, over the full range of simulated parameter values. This shows that the difference in thrust and torque values is arising solely due

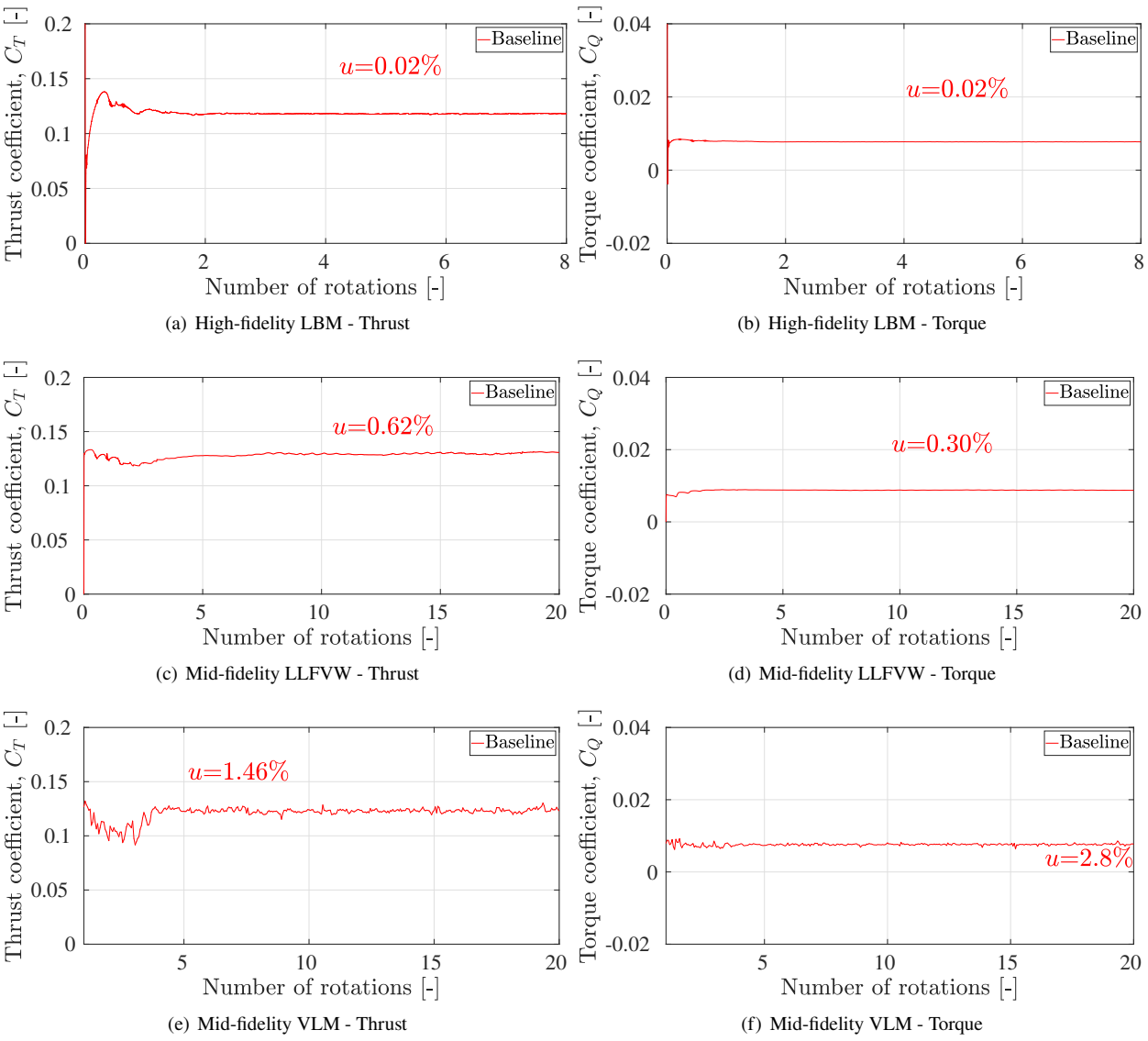

(a) High-fidelity LBM - Thrust

(b) High-fidelity LBM - Torque

(c) Mid-fidelity LLFVW - Thrust

(d) Mid-fidelity LLFVW - Torque

(e) Mid-fidelity VLM - Thrust

(f) Mid-fidelity VLM - Torque

Fig. 3 Statistical temporal convergence study for thrust coefficient C_T and torque coefficient C_Q using high-fidelity LBM and mid-fidelity LLFVW and VLM

to the different numerical methods used and different flow physics captured by each method.

Figures 7 report the results for thrust and torque variation with lateral velocity, for a constant freestream velocity of 10 m/s. For small values of lateral velocities, thrust and torque remain fairly constant with only a slight increase. The decrease in performance due to angular or skewed inflow is compensated for by the rise in effective total velocity. For 10 m/s, a significant increase in value is observed. In this case, the effect of an increase in total velocity experienced by the blades is more than the detrimental effect of skewed inflow, which translates to an increase in blade loading at all radial airfoil sections. LBM and LLFVW agree very well on thrust values but differ on torque values. VLM predicts the lowest values for thrust, whereas LBM predicts the lowest values for torque. And, similar to previous results, the difference in predicted values between different methods is constant across the full range of lateral velocities.

The performance offsets observed in the mid-fidelity solvers stem directly from their underlying aerodynamic assumptions. LLFVW employs a nonlinear lifting-line formulation coupled to an inviscid free-vortex wake and relies on XFOIL two-dimensional polars. Because these polars omit low-Reynolds-number laminar-bubble drag and rotational-stall augmentation, they over-predict sectional lift and under-predict profile drag. Moreover, the inviscid wake

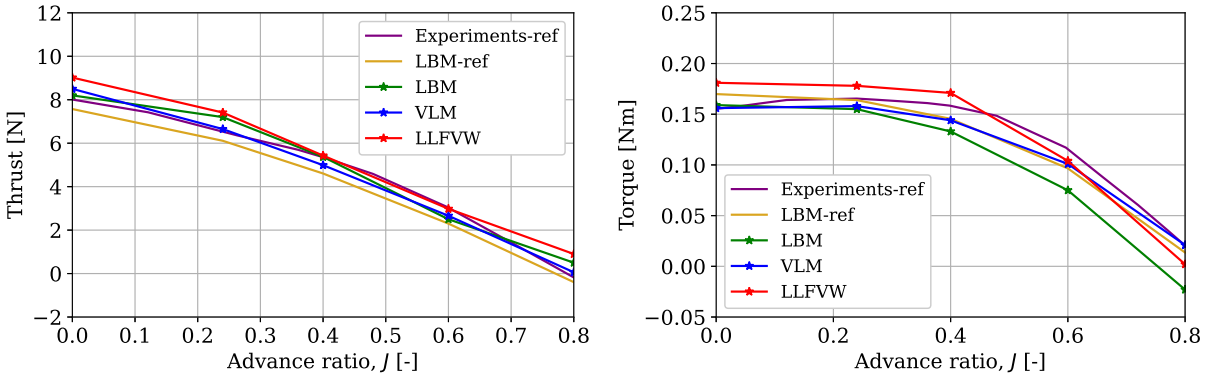

(a) Thrust (b) Torque

Fig. 4 Thrust coefficient C_T and torque coefficient C_Q comparison for different advance ratios with the baseline experimental results

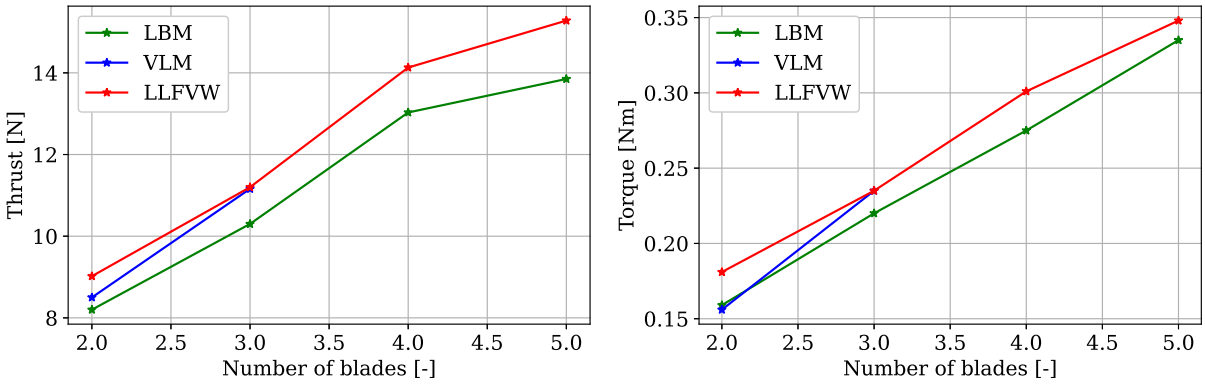

(a) Thrust (b) Torque

Fig. 5 Thrust coefficient C_T and torque coefficient C_Q comparison for different numbers of blades

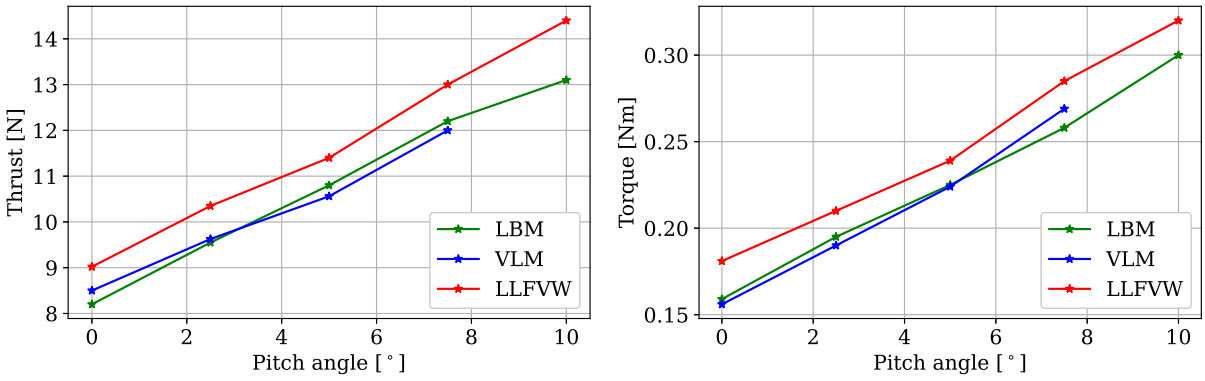

(a) Thrust (b) Torque

Fig. 6 Thrust coefficient C_T and torque coefficient C_Q comparison for different collective pitch angles

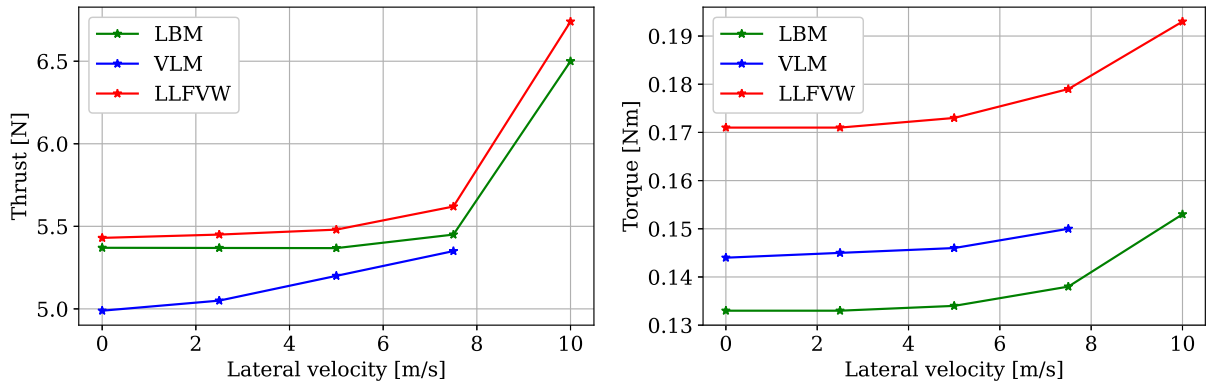

(a) Thrust

(b) Torque

Fig. 7 Thrust coefficient C_T and torque coefficient C_Q comparison for different values of lateral velocity, keeping freestream velocity constant at 10 m/s

conserves swirl energy instead of dissipating it, so induced losses are understated. Taken together, these effects lead LLFVW to report thrust and torque about 5–10% higher than the LBM benchmark.

By contrast, VLM (as implemented in VSPAero) represents each blade with an inviscid vortex lattice of limited chordwise resolution and convects a prescribed wake. The coarse panel spacing weakens the computed induced velocity, and the absence of viscous and stall corrections further reduces bound circulation. Consequently, VLM consistently predicts lower thrust and torque values by roughly 10–20% relative to LBM across almost all operating points.

The treatment of the wake amplifies these differences. LBM resolves viscous diffusion of tip vortices, swirl dissipation, and blade–vortex interaction, thereby accounting for the energy that is ultimately lost from the slipstream. LLFVW and VLM, which simply convect discrete vortex filaments without diffusion, miss these loss pathways. LLFVW therefore results in excess thrust, while VLM's already conservative prediction is compounded by an under-resolved inflow field. + Because the missing physics operate as nearly constant biases, both mid-fidelity methods still reproduce the correct performance gradients with advance ratio, blade number, pitch, and lateral velocity. A single calibration factor can align LLFVW downward or VLM upward to match experimental magnitudes while preserving sensitivities, making these tools attractive for rapid design sweeps. Nevertheless, regimes dominated by laminar-separation bubbles, dynamic stall, or intense wake interference will continue to require high-fidelity or empirically corrected analysis.

To gain further insight into flow physics and the differences between solution fidelities, flow field visualisations from the high-fidelity and mid-fidelity simulations were examined. Figure 8 compares the instantaneous wake structures predicted by LBM and LLFVW for the baseline propeller (2 blades, baseline pitch) in hover. The images show iso-surfaces of the λ_2 criterion, coloured by velocity magnitude, which effectively identify the vortex cores. In both simulations, one can observe the helical tip vortices shed from each blade tip, which trail downstream in a corkscrew pattern wrapping around the propeller. In the LBM solution, these tip vortices are very clearly defined near the blades and form coherent spiral rings in the wake. As they convect downstream, the LBM predicts that the vortices undergo wake contraction (the spiral radius decreases somewhat) and eventually fragment into smaller-scale vortices further downstream. This breakdown is caused by flow instabilities and the onset of turbulence in the wake, which leads to the vortices dissipating and mixing with the surrounding fluid. By a certain distance downstream, the once-coherent tip vortices have largely dissipated into a turbulent wake. These dynamically evolving vortex structures are responsible for phenomena such as blade-vortex interaction (BVI): as the propeller rotates, blades encounter the remnant vortices shed by preceding blades. In the LBM simulation, we indeed see evidence of rich small-scale vortex content, which would cause strong BVI and unsteady blade loading (the vortex-induced velocity impinging on the blades affects the pressure distribution). This manifests as the thrust and torque oscillations observed in the time histories, and it also means the real propeller would experience higher noise and fatigue loads due to these interactions.

The LLFVW wake visualisation reveals some important differences. The LLFVW model does capture the primary tip vortex spirals, and these vortices also wrap around the axis in a helical fashion. However, the mid-fidelity wake remains much more coherent and smooth compared to the LBM's turbulent wake. The LLFVW does not resolve the small-scale breakdown of the vortices; instead, the vortices persist as relatively intact filaments far downstream.

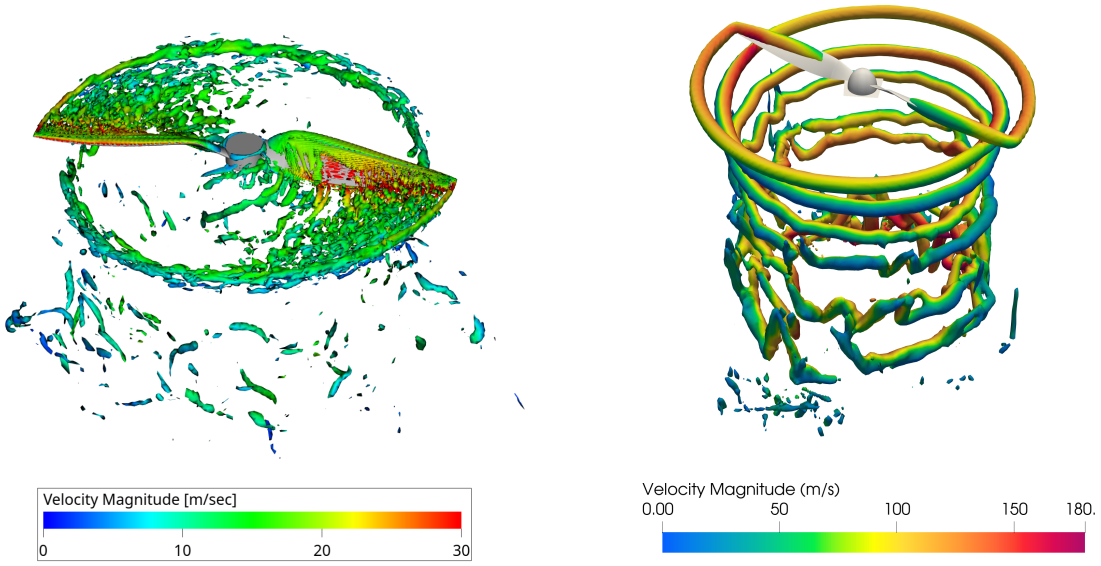

(a) High-fidelity LBM

(b) Mid-fidelity LLFVW

Fig. 8 Instantaneous 3D flowfield using iso-surfaces of the λ_2 criterion for vortices visualisation for the baseline propeller (2 blades, baseline pitch) in hover

There is little evidence of the smaller secondary vortex rings or turbulent eddies in the LLFVW visualisation – a direct consequence of its inviscid, lower-resolution approach. The fine-scale structures (small vortex loops, etc.) are absent. Consequently, the blade–vortex interaction in the LLFVW is weaker: the blades primarily interact with the smooth helical wake, without the high-frequency turbulent content present in the LBM case. This difference is one of the key reasons why LLFVW and LBM differ in predicted loads. In the LBM, the interaction of a blade with a fragmented, partially dissipated vortex (or a turbulent eddy) locally reduces lift or causes fluctuations, effectively reducing the time-averaged thrust slightly and increasing unsteady forces. The LLFVW, by convecting an idealised vortex, might actually impart a more consistent induced velocity on following blades (possibly even an overestimated induced velocity if vortex cores remain too strong), but without the dissipative losses.

Another perspective on the wake is given by Figure 9, which shows contours of the axial (streamwise) velocity in a vertical plane through the propeller axis. We compare the LBM and LLFVW results for two conditions: hover and forward flight (10 m/s). In hover, the propeller produces a classic propeller jet: air is accelerated downstream through the propeller disk, creating a high-speed jet along the axis. The LBM solution reveals a high-velocity core on the centreline just downstream of the propeller, with axial velocity well above the ambient (the peak likely occurs just behind the blades). As one moves radially outward from the axis, the LBM shows the velocity gradually decreasing. Importantly, the LBM predicts mixing at the edges of the slipstream, showing how ambient fluid is entrained and the jet diffuses outward with downstream distance. By a distance of roughly one diameter downstream, the axial velocity in the LBM case has diminished and spread, due to turbulent mixing in the shear layers.

The LLFVW hover result, in contrast, shows a sharper, more defined slipstream. The core high-velocity region remains narrow and persists further downstream with less reduction in magnitude immediately behind the propeller. The LLFVW's inviscid wake does include some induced velocity field, but it lacks turbulent diffusion, so the jet retains a more abrupt boundary between accelerated and quiescent flow. This aligns with expectations for an inviscid, free-vortex wake model – it convects the vortex sheet without dissipating energy. It should be noted that both models do predict the basic phenomenon of wake contraction – immediately after the propeller, the diameter of the slipstream is somewhat smaller than the prop disk.

In the forward-flight case (Figure 9 c,d), the flowfield is a superposition of the propeller-induced flow and the uniform freestream of 10 m/s. Upstream of the propeller, the flow is roughly 10 m/s everywhere (not shown in the figure). Downstream, both methods show an accelerated wake behind the prop. In the LBM case, for example, the highest velocities are on the order of 15-16 m/s in the wake. In the LLFVW, we see again a more uniform high-speed

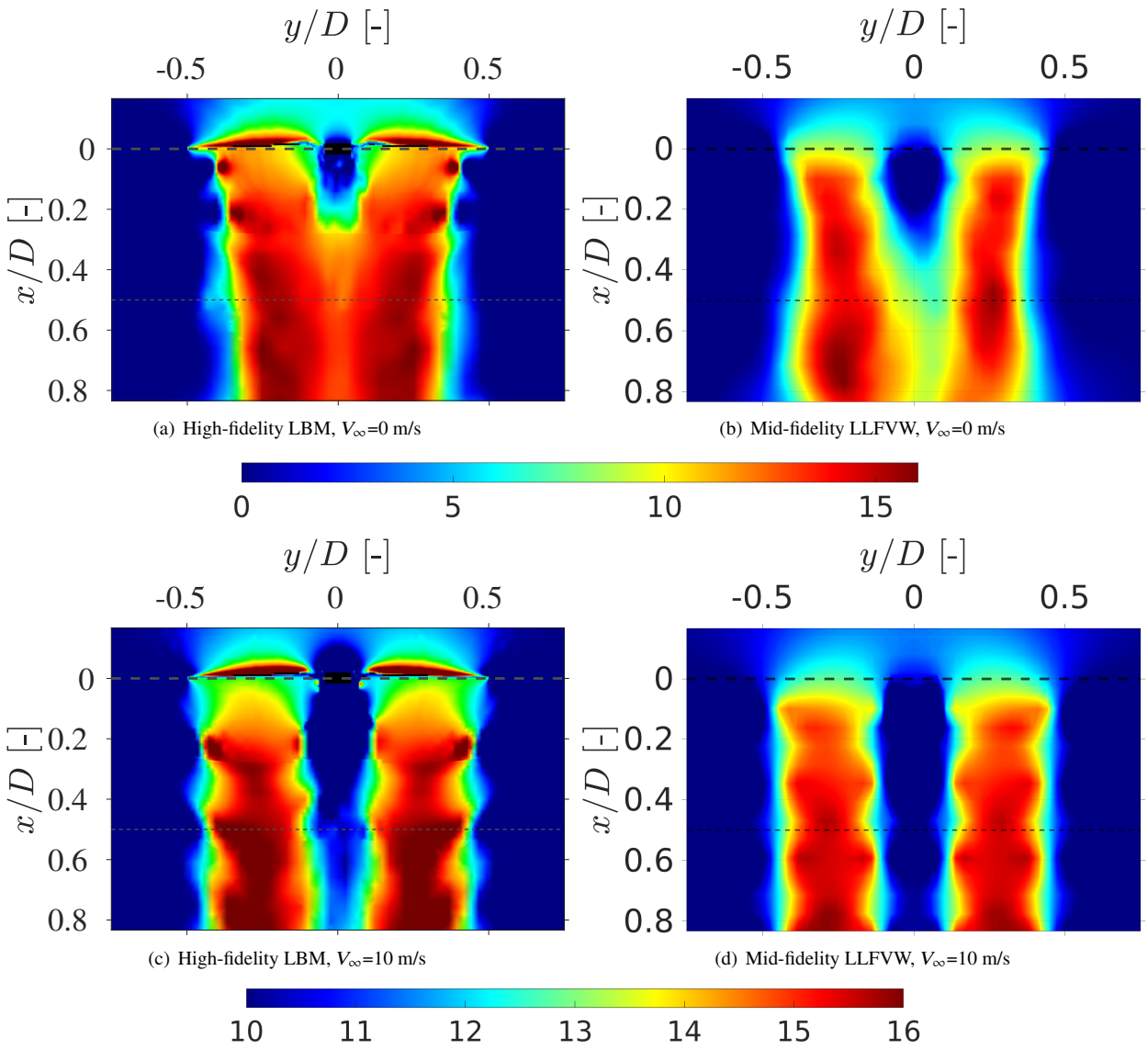

(a) High-fidelity LBM, V_∞=0 m/s

(b) Mid-fidelity LLFVW, V_∞=0 m/s

(c) High-fidelity LBM, V_∞=10 m/s

(d) Mid-fidelity LLFVW, V_∞=10 m/s

Fig. 9 2D contour plot for the streamwise velocities at the plane coinciding with the propeller axis; colorbar values are in m/s

core that persists. The freestream also causes the whole wake to be convected downstream – the high-speed region is stretched in the streamwise direction. Both models predict a slightly wider wake in forward flight compared to hover (since thrust and induced velocity are reduced in forward flight, so less streamtube contraction). The mixing in the LBM case is evident: the edges of the wake show a gradient where the high-speed propwash meets the 10 m/s freestream, indicating shear layers that will gradually mix out. The LLFVW, lacking turbulence, shows a more discrete slipstream boundary.

Overall, the flow visualisations highlight that the mid-fidelity LLFVW method captures the large-scale flow features (tip vortices, overall slipstream contraction and direction) reasonably well, but it fails to capture the finer details of vortex breakdown and turbulent diffusion present in the high-fidelity LBM results. This explains why LLFVW can consistently predict the correct trends and relative changes for different propeller designs (advance ratio, blade count, pitch, yaw, etc.), yet consistently deviates in absolute magnitude: it effectively assumes a cleaner, less dissipative flow than reality. The high-fidelity LBM, by resolving those small-scale structures, predicts slightly lower thrust (and different unsteady loads) because it accounts for the losses and interactions that the mid-fidelity model misses. In practical terms, one

could calibrate the mid-fidelity model (e.g. add a correction for induced power or drag) to reduce this bias, allowing it to match LBM or experimental data more closely. The present results suggest that such calibration would likely be a fixed offset or factor across the tested envelope since the LLFVW–LBM difference remained roughly constant for all cases. Thus, the multi-fidelity approach is viable: the LLFVW (and even the simpler VLM) can be used to rapidly explore propeller design changes and predict qualitative effects, and a high-fidelity LBM simulation can then be run for a few key points to adjust the predictions (if needed) and provide detailed insight into the flow mechanisms. The combination of both gives us the benefits of efficiency with mid-fidelity and accuracy with high-fidelity, enabling comprehensive propeller analyses with manageable computational expenses.

V. Conclusions and Recommendations

The present study investigates the aerodynamic prediction capabilities of three different multi-fidelity methods - high-fidelity Lattice Boltzmann Method (LBM), mid-fidelity Lifting Line Free Vortex Wake (LLFVW) and mid-fidelity Vortex Lattice Method (VLM). For a test case, a baseline propeller blade design, whose experimental results are available, is selected with 2 blades and 0.3 m diameter. A total of four design and operational parameters are investigated for a thorough investigation of the 3D design space of the propeller blade - advance ratio, number of blades, pitch angle and skewed inflow (lateral velocity).

The statistical temporal convergence in thrust and torque values for the baseline configuration is achieved after 4 rotor rotations using high-fidelity LBM, while it takes 8 rotor rotations using both mid-fidelity methods. Also, torque values exhibit faster convergence than thrust values using all the methods except VLM. The highest uncertainty in convergence values is found with mid-fidelity VLM values and the lowest is found with high-fidelity LBM values. Experimental validation is very good for high-fidelity LBM, for a range of advance ratios. But the LLFVW method predicts higher and the VLM method predicts lower values as compared to LBM, for both thrust and torque values. This is true for almost all design and operation parameters studied.

The thrust and torque results show a similar trend between all numerical methods used, with a constant difference in the predicted values over the complete range of design and operational parameters. This shows that the difference in thrust and torque values arises solely due to the different numerical methods used and different flow physics captured by each method. LLFVW, which uses inviscid lifting-line theory coupled with XFOIL polars, neglects laminar-bubble drag, rotational-stall effects, and swirl dissipation; it, therefore, over-predicts thrust/torque by roughly 5–10 %. VLM, formulated as a potential-flow lattice with coarse chordwise panels and a prescribed wake, under-resolves induced velocities and omits viscous lift, yielding 10–20 % lower loads than LBM.

3D iso-surfaces of the λ_2 criterion also show the difference in resolution of small-scale vortex structures between high-fidelity and mid-fidelity methods. The latter is unable to resolve those small structures in the 3D flowfield, as compared to the former, which leads to differences in capturing the blade-vortex interaction (BVI), causing a discrepancy in blade loading predicted by each method.

Computationally, LBM required ~2e4 CPU-hours for 12 revolutions, whereas LLFVW and VLM converged (after 8–10 revolutions) in a few CPU-hours — two to three orders of magnitude faster. A calibrated multi-fidelity workflow is therefore recommended: use LLFVW or VLM for rapid design sweeps, apply a single scale factor derived from sparse LBM or experimental anchors, and reserve LBM for final verification or regimes dominated by laminar-bubble, dynamic-stall, or detailed wake physics

Future studies should compare more multi-fidelity methods, such as - Vortex Panel Method, Blade Element Momentum Theory, high-fidelity Navier-Stokes method, Vortex Particle Method, etc. A surrogate model combining the results predicted by all the methods can be very beneficial, similar to a study done by Shubham et al. [47]. This framework can also be integrated into a web-based visual analytics framework [48] to better analyse the input data and results obtained.

Acknowledgments

This project has received funding from Innovate UK under Grant Agreement No 10003388.

References

[1] Casalino, D., Grande, E., Romani, G., Ragni, D., and Avallone, F., "Definition of a benchmark for low Reynolds number propeller aeroacoustics," *Aerospace Science and Technology*, Vol. 113, 2021, p. 106707.

[2] Adkins, K. A., "Urban flow and small unmanned aerial system operations in the built environment," *International Journal of Aviation, Aeronautics, and Aerospace*, Vol. 6, No. 1, 2019, p. 10.

[3] Deters, R. W., *Performance and slipstream characteristics of small-scale propellers at low Reynolds numbers*, University of Illinois at Urbana-Champaign, 2014.

[4] Nagy, A. B., Delfs, J., and Bennett, G. J., "Aeroacoustics research in Europe: The CEAS-ASC report on 2020 & 2021 highlights," *Journal of Sound and Vibration*, Vol. 534, 2022, p. 117002.

[5] Atassi, H. M., *Unsteady aerodynamics, aeroacoustics, and aeroelasticity of turbomachines and propellers*, Springer Science & Business Media, 2012.

[6] MacNeill, R., and Verstraete, D., "Blade element momentum theory extended to model low Reynolds number propeller performance," *The Aeronautical Journal*, Vol. 121, No. 1240, 2017, pp. 835–857.

[7] Hang, L. C., Rosli, N. A. N., Ab Wahid, M., Othman, N., Mat, S., and Zain, M. Z. M., "CFD Analysis on Propeller at Varying Propeller Disc Angle and Advance Ratio," *Journal of Advanced Research in Fluid Mechanics and Thermal Sciences*, Vol. 96, No. 1, 2022, pp. 82–95.

[8] Toman, U. T., Hassan, A.-K. S., Owis, F. M., and Mohamed, A. S., "Blade shape optimization of an aircraft propeller using space mapping surrogates," *Advances in Mechanical Engineering*, Vol. 11, No. 7, 2019, p. 1687814019865071.

[9] Di Pasquale, D., Tarun, T., Shubham, S., Prince, S., and Proenca, A., "COMPUTATIONAL ANALYSIS ON THE EFFECTS OF LEADING EDGE TUBERCLES ON THE PERFORMANCE OF ROTATING PROPELLER," *34th Congress of the International Council of the Aeronautical Sciences*, 2024.

[10] Shubham, S., Spinelli, A., and Kipouros, T., "Multi-fidelity multi-disciplinary optimisation of propeller design by visual analytics," *The Eurographics Association*, 2024.

[11] Marten, D., Wendler, J., Pechlivanoglou, G., Nayeri, C. N., and Paschereit, C. O., "QBLADE: an open source tool for design and simulation of horizontal and vertical axis wind turbines," *International Journal of Emerging Technology and Advanced Engineering*, Vol. 3, No. 3, 2013, pp. 264–269.

[12] Thambidurai Arasi, T. R., Shubham, S., and Ianakiev, A., "Effect of Blade Shape on Aerodynamic and Aeroacoustic characteristics of Vertical Axis Wind Turbines using mid-fidelity and high-fidelity methods," *AIAA SCITECH 2024 Forum*, 2024, p. 1488.

[13] Shubham, S., Naik, K., Sachar, S., and Ianakiev, A., "Performance analysis of low Reynolds number vertical axis wind turbines using low-fidelity and mid-fidelity methods and wind conditions in the city of Nottingham," *Energy*, Vol. 279, 2023, p. 127904.

[14] Shubham, S., "A multi-fidelity approach for aerodynamics and aeroacoustics of vertical axis wind turbines," Ph.D. thesis, Nottingham Trent University (United Kingdom), 2024.

[15] Marten, D., Bianchini, A., Pechlivanoglou, G., Balduzzi, F., Nayeri, C. N., Ferrara, G., Paschereit, C. O., and Ferrari, L., "Effects of airfoil's polar data in the stall region on the estimation of Darrieus wind turbine performance," *Journal of Engineering for Gas Turbines and Power*, Vol. 139, No. 2, 2017.

[16] Balduzzi, F., Marten, D., Bianchini, A., Drofelnik, J., Ferrari, L., Campobasso, M. S., Pechlivanoglou, G., Nayeri, C. N., Ferrara, G., and Paschereit, C. O., "Three-dimensional aerodynamic analysis of a Darrieus wind turbine blade using computational fluid dynamics and lifting line theory," *Journal of Engineering for Gas Turbines and Power*, Vol. 140, No. 2, 2018.

[17] Van Garrel, A., "Development of a wind turbine aerodynamics simulation module," 2003.

[18] Marten, D., "QBlade Guidelines v0. 95," *Technical University of Berlin, Berlin, Germany*, 2016.

[19] Marten, D., Lennie, M., Pechlivanoglou, G., Nayeri, C. N., and Paschereit, C. O., "Implementation, optimization, and validation of a nonlinear lifting line-free vortex wake module within the wind turbine simulation code qblade," *Journal of Engineering for Gas Turbines and Power*, Vol. 138, No. 7, 2016.

[20] Marten, D., Pechlivanoglou, G., Navid Nayeri, C., and Oliver Paschereit, C., "Nonlinear lifting line theory applied to vertical axis wind turbines: Development of a practical design tool," *Journal of Fluids Engineering*, Vol. 140, No. 2, 2018.

[21] Bergami, L., and Gaunaa, M., "ATEFlap Aerodynamic Model, a dynamic stall model including the effects of trailing edge flap deflection," 2012.

[22] Wendler, J., Marten, D., Pechlivanoglou, G., Nayeri, C. N., and Paschereit, C. O., "An unsteady aerodynamics model for lifting line free vortex wake simulations of hawt and vawt in qblade," *Turbo Expo: Power for Land, Sea, and Air*, Vol. 49873, American Society of Mechanical Engineers, 2016, p. V009T46A011.

[23] "Open Vehicle Sketch Pad (OpenVSP)," Available online at: `http://www.openvsp.org`, 2025. Accessed: 23 Jun 2025.

[24] Katz, J., *Low-speed aerodynamics*, Cambridge University Press, 2001.

[25] Leishman, G. J., *Principles of helicopter aerodynamics with CD extra*, Cambridge university press, 2006.

[26] Shubham, S., Avallone, F., Brandetti, L., Wright, N., and Ianakiev, A., "Effect of struts and central tower on aerodynamics and aeroacoustics of vertical axis wind turbines using mid-fidelity and high-fidelity methods," *AIAA SCITECH 2024 Forum*, 2024, p. 1485.

[27] Gourdain, N., Jardin, T., Serre, R., Prothin, S., and Moschetta, J.-M., "Application of a lattice Boltzmann method to some challenges related to micro-air vehicles," *International Journal of Micro Air Vehicles*, Vol. 10, No. 3, 2018, pp. 285–299.

[28] Grande, E., Shubham, S., Avallone, F., Ragni, D., and Casalino, D., "Computational aeroacoustic study of co-rotating rotors in hover," *Aerospace Science and Technology*, Vol. 153, 2024, p. 109381.

[29] Avallone, F., van den Ende, L., Li, Q., Ragni, D., Casalino, D., Eitelberg, G., and Veldhuis, L., "Aerodynamic and aeroacoustic effects of swirl recovery vanes length," *Journal of Aircraft*, Vol. 56, No. 6, 2019, pp. 2223–2235.

[30] Casalino, D., Hazir, A., and Mann, A., "Turbofan broadband noise prediction using the lattice Boltzmann method," *AIAA Journal*, Vol. 56, No. 2, 2018, pp. 609–628.

[31] Nardari, C., Casalino, D., Polidoro, F., Coralic, V., Lew, P.-T., and Brodie, J., "Numerical and experimental investigation of flow confinement effects on UAV rotor noise," *25th AIAA/CEAS Aeroacoustics Conference*, 2019, p. 2497.

[32] Shubham, S., Kipouros, T., Dash, S., and Ianakiev, A., "Uncertainty propagation and management of mixed uncertainties for multi-fidelity multi-disciplinary analysis of propeller with different blade sweep," *AIAA SCITECH 2024 Forum*, 2024, p. 1487.

[33] Succi, S., *The lattice Boltzmann equation for fluid dynamics and beyond*, 1st ed., Clarendon Press, Oxford, 2001.

[34] Shan, X., Yuan, X.-F., and Chen, H., "Kinetic theory representation of hydrodynamics: a way beyond the Navier–Stokes equation," *Journal of Fluid Mechanics*, Vol. 550, 2006, pp. 413–441. https://doi.org/10.1017/S0022112005008153, URL http://www.journals.cambridge.org/abstract_S0022112005008153.

[35] Chen, S., and Doolen, G., "Lattice Boltzmann method for fluid flows," *Annual Review of Fluid Mechanics*, Vol. 30, No. 1, 1998, pp. 329–364. https://doi.org/10.1146/annurev.fluid.30.1.329, URL http://www.annualreviews.org/doi/10.1146/annurev.fluid.30.1.329.

[36] Chen, H., Chen, S., and Matthaeus, W., "Recovery of the Navier-Stokes equations using a lattice-gas Boltzmann method," *Physical Review A*, Vol. 45, No. 8, 1992, pp. R5339–R5342. https://doi.org/10.1103/PhysRevA.45.R5339, URL https://link.aps.org/doi/10.1103/PhysRevA.45.R5339.

[37] Chen, H., Zhang, R., and Gopalakrishnan, P., "Lattice Boltzmann Collision Operators Enforcing Isotropy and Galilean Invariance," , 8 2015. URL https://patents.google.com/patent/US20150356217A1/en.

[38] Yakhot, V., and Orszag, S., "Renormalization group analysis of turbulence. I. Basic theory," *Journal of Scientific Computing*, Vol. 1, No. 1, 1986, pp. 3–51. https://doi.org/10.1007/BF01061452, URL http://link.springer.com/10.1007/BF01061452.

[39] Teixeira, C., "Incorporating Turbulence Models into the Lattice-Boltzmann Method," *International Journal of Modern Physics C*, Vol. 09, No. 08, 1998, pp. 1159–1175. https://doi.org/10.1142/S0129183198001060, URL http://www.worldscientific.com/doi/abs/10.1142/S0129183198001060.

[40] Wilcox, D., *Turbulence modelling for CFD (Third Edition)*, DCW Industries, Incorporated, 2006.

[41] Launder, B., and Spalding, D., "The numerical computation of turbulent flows," *Computer Methods in Applied Mechanics and Engineering*, Vol. 3, No. 2, 1974, pp. 269–289. https://doi.org/10.1016/0045-7825(74)90029-2, URL http://www.sciencedirect.com/science/article/pii/0045782574900292.

[42] Drela, M., "XFOIL: An analysis and design system for low Reynolds number airfoils," *Low Reynolds number aerodynamics*, Springer, 1989, pp. 1–12.

[43] Montgomerie, B., "Methods for root effects, tip effects and extending the angle of attack range to±180, with application to aerodynamics for blades on wind turbines and propellers," *FOI, Swedish Defence Research Agency, Stockholm, Sweden, Report No. FOI*, 2004.

[44] Shubham, S., Wright, N., and Ianakiev, A., "Application of Richardson extrapolation method to aerodynamic and aeroacoustic characteristics of low Reynolds number vertical axis wind turbines," *28th AIAA/CEAS Aeroacoustics 2022 Conference*, 2022, p. 3022.

[45] Shubham, S., Wright, N., Avallone, F., and Ianakiev, A., "Aerodynamic and aeroacoustic investigation of vertical axis wind turbines with different number of blades using mid-fidelity and high-fidelity methods," *AIAA AVIATION 2023 Forum*, 2023, p. 3642.

[46] Shubham, S., "Computational Aeroacoustic Investigation of Co-rotating rotors for Urban Air Mobility," 2020.

[47] Shubham, S., and Sharma, A., "A multi-dimensional machine learning framework for superior propeller design choices," *AIAA Aviation Forum*, 2025.

[48] Shubham, S., Spinelli, A., and Kipouros, T., "Visual Analytics Framework for Multi-Disciplinary Multi-Objective Optimisation of Aircraft Design," *Available at SSRN 5114731*, 2025.

https://dspace.org/

Multi-fidelity investigation of low-reynolds number propeller for different design parameters

Sharma, Ankit; Shubham, Shubham; Riaz, Atif; Ianakiev, Anton

2025-07-29
American Institute of Aeronautics and Astronautics (AIAA)
https://doi.org/10.2514/6.2025-3693
Sharma A, Shubham S, Riaz A, Ianakiev A. (2025) Multi-fidelity investigation of low-reynolds number propeller for different design parameters. In: AIAA Aviation Forum and Ascend 2025, 21-25 July 2025, Las Vegas, USA, Article number 2025-3693

Downloaded from a DSpace repository. https://dspace.org/